euspen's 26th International Conference & Exhibition, Krakow, PL, June 2026
www.euspen.eu

Aerostatic journal bearing as a capacitive sensor for in-situ radial rotor position measurement

Petteri Haverinen[1], Mikael Miettinen[1], Raine Viitala[1]

[1]*Aalto University*

Petteri.haverinen@aalto.fi

Abstract
Aerostatic journal bearings are low friction bearings, like plain bearings or bushings, which have a high-pressure gas film between a shaft and the bearing. In cases, where the restrictor of the bearing is electrically conductive material, such as porous graphite, it is possible to measure the average thickness of the air film using capacitive sensing. To measure runout and angular velocity of the shaft, the bearing can be split into multiple sections, where the thickness of the air film is measured between each of the sections and the shaft.
Previous methods have utilized external sensors in conjunction with journal bearings to characterize the parameters of the bearing, such as runout. However, little work has been done to utilize the bearing as a sensor.
In the present study, a porous journal bearing with four electrically insulated rigid bearing pads was developed and characterized. The bearing used graphite restrictors, which were also used as electrodes for the capacitive displacement sensor. Adjacent external capacitive sensors were used to verify the accuracy of the proposed method. A rigid rotor supported by the investigated bearing was rotated with an unbalanced mass mounted to the rotor to induce runout. The shaft position was measured with the integrated sensors and adjacent external reference sensors. Results show that the accuracy of the proposed method is 326 nm, highlighting the feasibility of integrated capacitive sensing in aerostatic bearing systems.

Gas bearings, Journal bearings, capacitive sensing, runout

1. Introduction

Porous aerostatic bearings are externally pressurized cylindrical bearings, sharing similarities with plain bearings [1]. However, instead of an oil film, the pressurized gas produces a thin air gap between the rotating shaft and the bearing. This gap allows for low-friction motion, ideal for high speed or high accuracy applications [2].

One of such use cases is in high-speed precision spindles, where the rotating toolholder is supported by a journal bearing in conjunction with two thrust bearings, forming an H-spindle. As the tool contacts the workpiece, the spindle experiences load which may induce motion to the spindle itself [3]. Furthermore, the spindle shaft tolerances in cylindricity and roundness has been observed to cause unbalanced force produced by the air gap causing instability in the spindle [4].

To monitor and account in real time for the radial motion of the shaft, a measurement system is required to measure the shaft position in real time. Previous works have utilized external sensors to measure the spindle motion [4, 5]. However, previous developments in utilizing aerostatic bearings as sensors [6] have pointed to developing a journal bearing, which can measure the air gap thickness at sections to measure the shaft position.

The present work investigates a novel aerostatic journal bearing with split restrictor to measure the air gap and the shaft position. A journal bearing with a sensor functionality was developed in conjunction with measurement electronics and the performance was experimentally validated with unbalanced mass to induce runout in the bearing.

2. Methods

The present work developed a porous journal bearing with a split restrictor. The radial position of the shaft was measured with the electrodes using capacitive sensing. The measurement electronics were developed and verified against reference sensors.

The shaft was rotated at different angular velocities and with an eccentric shaft. The radial position of the shaft was measured with the bearing and reference sensors. The output of the developed sensor was fitted with the data from the reference sensors.

2.1. Investigated bearing

The bearing was constructed in two halves with alignment pins and bolt connection. This allowed for the aerostatic pads to be adhered to the body and turned into the final geometry at a later stage. The bearing body was manufactured from hard-anodized aluminium to prevent electrical contact from the bearing pads to the body. The journal bearing pads were manufactured from porous graphite and adhered to the bearing body with epoxy. After the epoxy had cured, the bearing was mounted on a lathe, and the inside was bored to 39.995 mm and lapped with a 40 mm hydraulic cylinder rod for final tolerance.

Each bearing pad had an electrical feedthrough and a port for pressure supply. The electrical feedthroughs consisted of a nylon bolt with a 1 mm hole to accommodate a 1 mm tig welding rod, which was fixed in place with cyanoacrylate adhesive.

The bearing consumed air at 4 l/min at 0.4 MPa operating pressure with the shaft installed. The short circuit flow of the bearing was 6.4 l/min.

The main dimensions and construction of the bearing are presented in figure 1.

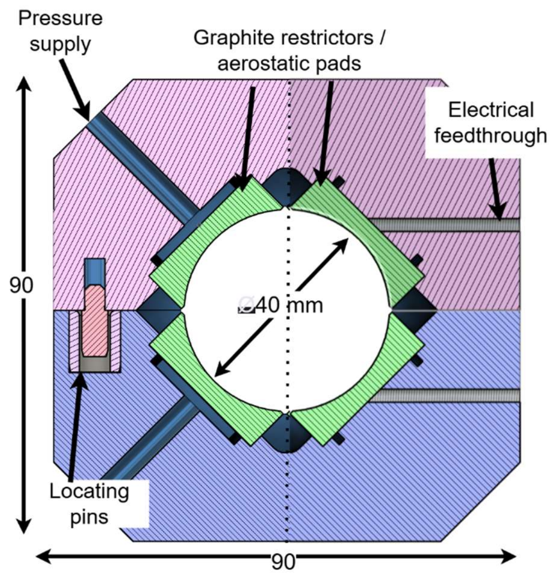

Figure 1. Diagram of the investigated bearing. Each corner had a pressure supply port with M5 thread. The picture is a section from front with two section depths at the dotted line. The locating pins were mounted to ensure alignment with one side having a cylinder pin and the other a diamond shaped pin. The electrical feedthroughs were 2.5 mm in diameter piercing to the graphite off to the side from the pressure supply.

2.2. Measurement electronics

For the electrodes to measure the position of the shaft, measurement electronics are required. While multiple methods to measure capacitance exist [7], the present work utilized a capacitance-to-voltage converter circuit.

Each electrode had a capacitance in respect to measurement ground through the rotating shaft due to the air gap [8]. As the air gap decreases, the capacitance of the adjacent electrode increases. The change in capacitance was measured by measuring current through the capacitor. A sine wave excitation signal with 10 MHz frequency and 10 V amplitude was supplied to each electrode through a resistor. The voltage drop over the capacitor was rectified with a diode and a low-pass filter set to 16 kHz. The potential difference over opposing capacitors (electrodes) was amplified with a difference amplifier. The position in each axis was therefore represented by the output voltage of the amplifier ranging from -5 to +5 V in respect to the measurement ground. The circuit diagram is presented in figure 2.

The circuit response in relation to the distance is linear. Assuming, that the time constant is large, the voltage drop over opposing capacitors (Figure 2. C1 & C2, C3 & C4) can be approximated as:

$$U_c \approx \frac{U_s}{j\omega RC}$$

Where U_s is the amplitude of the excitation signal, R is the resistor in series with the capacitor and ω is angular velocity of the excitation signal. The output in the circuit is the difference between the voltage drops over the opposing capacitors as:

$$U_{out} = U_{C1} - U_{C2}$$

The capacitances are inversely proportional to each other. As the distance between the shaft and the electrode of C1 decreases its capacitance increases, while simultaneously the distance between the shaft and electrode of C2 increases, its capacitance decreases. This relationship can be expressed as:

$$d_{C1} = d_0 - \Delta d$$
$$d_{C2} = d_0 + \Delta d$$

The capacitance relating to the distances is:

$$C = \varepsilon_0 \varepsilon_r \frac{A}{d}$$

Where d is the distance d_{C1} or d_{C2}, A is the surface area of the electrode, ε_0 is the permittivity of free space and ε_r is the relative permittivity of air, which is approximately 1 [9].

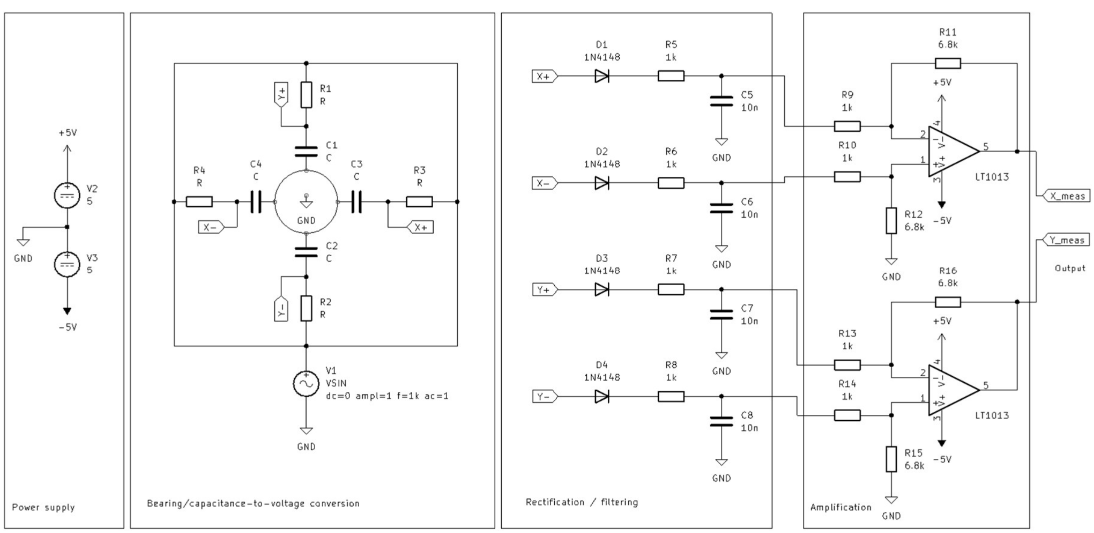

Figure 2. Schematic of the measurement circuit. The capacitance formed between the air gap and each electrode was converted to voltage using an RC circuit with a sinusoidal excitation at 10 MHz and 10 V peak-to-peak amplitude. The voltage drop across each capacitor was rectified and filtered with a low pass filter. The voltage output (X_meas & Y_meas) was the difference across the opposing capacitors amplified by gain of 3.3.

By combining these equations, the response of the circuit before the amplifier is:

$$U_{out} = \frac{2U_s \Delta d}{\omega R \varepsilon_0 \varepsilon_r A}$$

From the equation, it is evident that the output increases linearly to the change in distance:

$$U_{out} \propto \Delta d$$

2.3. Experiments

The bearing was mounted on a testbench with a 40 mm diameter shaft. The shaft was loaded against a sphere on one end with a magnetic preload on the opposing end. The spherical contact allowed for electrical grounding the shaft while keeping the contact friction relatively low. The bearing was pressurized at 0.4 MPa. External reference sensors were used at 45 degrees from the bearing electrodes to calibrate the integrated sensor and to verify the results.

The shaft was rotated with pressurized air, and its radial position was measured with the external reference sensor in conjunction with the output voltage from the measurement circuit. The experiment was repeated with an unbalanced mass produced by attaching magnets to the shaft. The mass of each magnet was 30 grams. The radius of the masses was 14 mm, producing an unbalance of $U = 840g \cdot mm$.

To measure the output of the reference sensors and the voltage form the measurement circuit, a NI-USB6001 was used. Each measurement lasted 20 seconds at 10 ks/s sampling rate. The test setup is presented in figure 3.

Due to the axial offset between the reference sensors and the geometric deviations in the shaft, only the low frequency components relating to the mean displacement of the shaft were analysed from the measurement data. The measured data was passed through at a 20 Hz low pass filter.

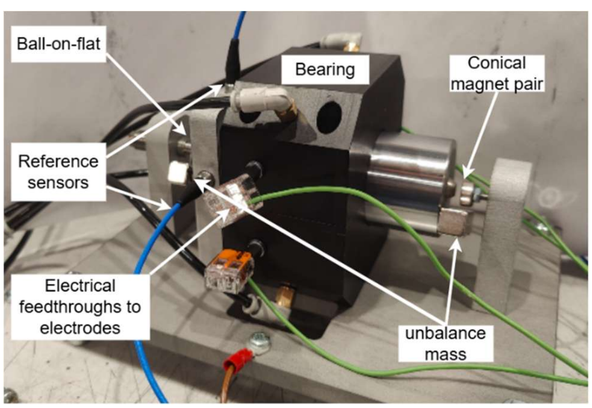

Figure 3. Experiment setup. The bearing was mounted on a steel plate with bolts, supported by a spherical ball-on-flat contact on one end and by opposing conical magnets on one end. The unbalance masses were mounted on same radial location on opposing ends of the shaft.

3. Results and Discussion

The shaft had an average rotational speed of 1165 RPM. The rotational speed varied since the shaft was accelerated by compressed air. The rotational speed was derived from the output of the reference sensor signal. The rotational speed measurement is presented in figure 4. The results are presented in the window of 8-10 second, where the rotational speed had lowest amount of variation.

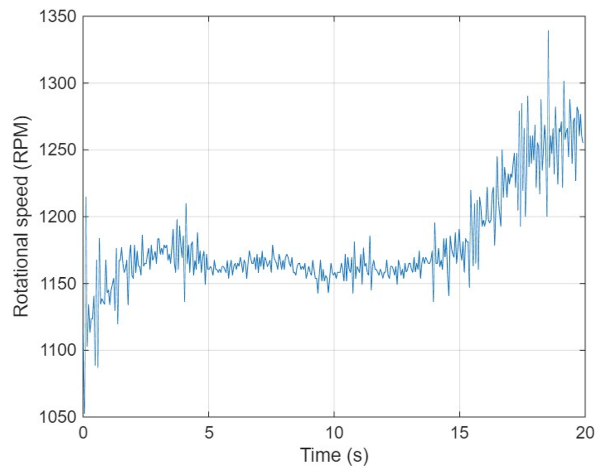

Figure 4. Rotational speed of the shaft. The variation in the rotational speed was a result of using compressed air to accelerate the shaft.

The sensor output was linear in respect to the displacement measured by the reference sensors. The phase of the reference sensor signal was rotated to match the phase of the measurement electronics signal, since the reference sensors were offset by 45 degrees. The sensor output in respect to the reference sensor and the used fit for scaling the output are presented in figure 5.

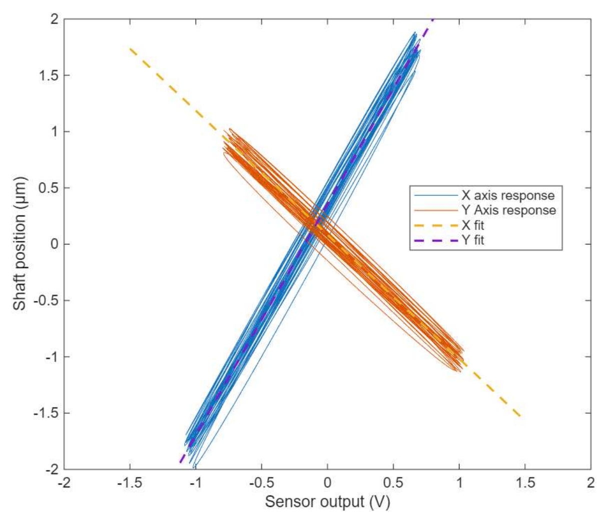

Figure 5. Output of the measurement electronics vs the shaft position measured by the reference sensors. Blue is the X axis output, red is the Y axis, yellow dotted line is the X axis fit and purple is the Y axis fit. The fitted lines were:

$f_x(U_x) = -1.102\ U_x + 0.084$ and $f_y(U_y) = 2.051\ U_y + 0.355$

The trajectory of the shaft during the measurement is presented in figure 6, where A) presents the trajectory as seen by the measurement electronics, B) presents the measurement electronics output scaled to micrometres with the reference measurements overlayed on top.

The sensor output varied from -1.087 V to 0.707 V on Y axis and from -0.797 V to 1.037 V on X axis. The maximum deviation on Y axis after fitting the sensor data to the reference sensor data was 326 nm and on X axis 229 nm, corresponding to 8.4% and 10.6% relative error.

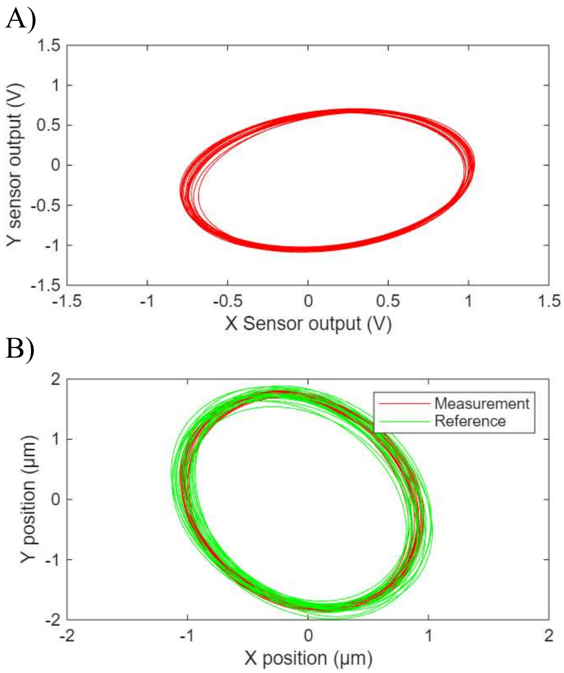

Figure 6. A) Orbit as a voltage from the measurement electronics, B) orbit from the reference sensor and the developed sensor. The shaft had a displacement of 2.167 µm on X axis and 3.873 µm on Y axis.

The reference sensor measurement had more variation, than the developed sensor. A major factor impacting the result is that the reference sensor does not measure directly from inside of the bearing. The sensors were mounted 10 mm away from the bearing, thus being further away from the support. Moreover, future work will incorporate the measurement electronics in a shielded enclosure to reduce the effect of electromagnetic noise on the measurements.

While the present work acts a as a solid proof-of-concept, the accuracy reported is not suitable for high precision spindles. The measurement accuracy must be in nanometre scale as the error motion in these spindles can be in tens of nanometres [10].

Future work must address the higher frequency components on the measured signal. The present work provides a solid foundation for calibrating and characterising a porous aerostatic journal bearing with capacitive displacement sensor capability but has yet to address the dynamic range due to low-pass filtering used. The high frequency components due to surface geometry remains unvalidated and must be further researched.

5. Conclusions

The present work developed and experimentally investigated a novel porous aerostatic journal bearing acting as a capacitive displacement sensor for shaft radial position measurement. The shaft was unbalanced with an unbalance of $U = 840g \cdot mm$ and rotated at 1165 RPM. The resulting orbit was measured with external capacitive reference sensors and with the bearing using developed measurement electronics.

The sensor had a maximum deviation of 326 nm on Y axis, which was 8.4% relative error and 229 nm deviation on the X axis with 10.6% relative error respectively.

References

[1] Farid Al-Bender. Air bearings : theory, design and applications. Hoboken, Nj, Usa: Wiley; 2020.

[2] Gao Q, Chen W, Lu L, Huo D, Cheng K. Aerostatic bearings design and analysis with the application to precision engineering: State-of-the-art and future perspectives. Tribology International [Internet]. 2019 Jul 1 [cited 2023 Mar 30];135:1–17. Available from: https://www.sciencedirect.com/science/article/pii/S0301679X19300830

[3] Kim JH, Chang HK, Han DC, Jang DY, Oh SI. Cutting Force Estimation by Measuring Spindle Displacement in Milling Process. CIRP Annals. 2005;54(1):67–70.

[4] Zhang, Guoqing, et al. "Rotation Accuracy Analysis of Aerostatic Spindle Considering Shaft's Roundness and Cylindricity." Applied Sciences, vol. 11, no. 17, 27 Aug. 2021, p. 7912, https://doi.org/10.3390/app11177912. Accessed 19 Feb. 2023.

[5] Miao H, Li C, Wang C, Xu M, Zhang Y. The vibration analysis of the CNC vertical milling machine spindle system considering nonlinear and nonsmooth bearing restoring force. Mechanical Systems and Signal Processing. 2021 Dec;161:107970.

[6] Haverinen P, Miettinen M, Viitala R. Porous aerostatic bearing with integrated air gap height measurement. Measurement [Internet]. 2025 Jun 27;256:118128. Available from: https://www.sciencedirect.com/science/article/pii/S0263224125014873#b1

[7] Kanoun O, Kallel AY, Fendri A. Measurement Methods for Capacitances in the Range of 1 pF–1 nF: A review. Measurement. 2022 May;195:111067.

[8] Haverinen P, Miettinen M, Harding L, Vainio V, Leutonen O, Theska R, et al. Integrated capacitive measurement of air gap height in aerostatic bearings [Internet]. 2024 [cited 2026 Feb 2]. Available from: https://www.euspen.eu/knowledge-base/ICE24211.pdf

[9] Hector LG, Schultz HL. The Dielectric Constant of Air at Radiofrequencies. Physics. 1936 Apr;7(4):133–6.

[10] Knapp B, Arneson D. Dynamic Characterization of a Micro-machining Spindle. Wiscedu [Internet]. 2026 [cited 2026 Feb 2]; Available from: http://digital.library.wisc.edu/1793/68586